Letter

Annihilation of topological solitons in magnetism with spin-wave burst finale: Role of nonequilibrium electrons causing nonlocal damping and spin pumping over ultrabroadband frequency range

Marko D. Petrović,[1] Utkarsh Bajpai,[1] Petr Plecháč,[2] and Branislav K. Nikolić[1,*]
[1]*Department of Physics and Astronomy, University of Delaware, Newark, Delaware 19716, USA*
[2]*Department of Mathematical Sciences, University of Delaware, Newark, Delaware 19716, USA*

(Received 9 August 2019; revised 17 June 2021; accepted 21 June 2021; published 14 July 2021)

We not only reproduce a burst of short-wavelength spin waves (SWs) observed in a recent experiment [S. Woo *et al.*, Nat. Phys. **13**, 448 (2017)] on magnetic-field-driven annihilation of two magnetic domain walls (DWs) but, furthermore, we predict that this setup additionally generates *highly unusual* pumping of electronic spin currents in the absence of any bias voltage. Prior to the instant of annihilation, their power spectrum is *ultrabroadband*, so they can be converted into rapidly changing in time charge currents, via the inverse spin Hall effect, as a source of THz radiation of *bandwidth* $\simeq$27 THz where the lowest frequency is controlled by the applied magnetic field. The spin pumping stems from time-dependent fields introduced into the quantum Hamiltonian of electrons by the classical dynamics of localized magnetic moments (LMMs) comprising the domains. The pumped currents carry spin-polarized electrons which, in turn, exert *backaction* on LMMs in the form of nonlocal damping which is more than twice as large as conventional local Gilbert damping. The nonlocal damping can substantially modify the spectrum of emitted SWs when compared to widely used micromagnetic simulations where conduction electrons are completely *absent*. Since we use a fully microscopic (i.e., Hamiltonian-based) framework, self-consistently combining time-dependent electronic nonequilibrium Green functions with the Landau-Lifshitz-Gilbert equation, we also demonstrate that previously derived phenomenological formulas miss ultrabroadband spin pumping while underestimating the magnitude of nonlocal damping due to *nonequilibrium electrons*.

DOI: 10.1103/PhysRevB.104.L020407

Introduction. The control of the domain wall (DW) motion [1–3] within magnetic nanowires by magnetic field or current pulses is both a fundamental problem for nonequilibrium quantum many-body physics and a building block of envisaged applications in digital memories [4], logic [5], and artificial neural networks [6]. Since DWs will be closely packed in such devices, understanding the interaction between them is a problem of great interest. [7] For example, head-to-head or tail-to-tail DWs—illustrated as the left (L) or right (R) noncollinear texture of localized magnetic moments (LMMs), respectively, in Fig. 1—behave as free magnetic monopoles carrying topological charge. [8] The topological charge (or the winding number) $Q \equiv -\frac{1}{\pi}\int dx\, \partial_x \phi$, associated with winding of LMMs as they interpolate between two uniform degenerate ground states with $\phi = 0$ or $\phi = \pi$, is opposite for adjacent DWs, such as $Q_L = -1$ and $Q_{\rm R} = +1$ for DWs in Fig. 1. Thus, long-range attractive interaction between DWs can lead to their *annihilation*, resulting in the ground state without any DWs. [9–12] This is possible because total topological charge remains conserved, $Q_L + Q_{\rm R} = 0$. The *nonequilibrium dynamics* [13] triggered by annihilation of topological solitons is also of great interest in many other fields of physics, such as cosmology [14], gravitational waves [15], quantum [13] and string field [16] theories, liquid crystals [17], and Bose-Einstein condensates [18,19].

A recent experiment [20] has monitored annihilation of two DWs within a metallic ferromagnetic nanowire by observing an intense burst of spin waves (SWs) at the moment of annihilation. Thus generated large-amplitude SWs are dominated by exchange, rather than dipolar, interaction between LMMs and are, therefore, of short wavelength. The SWs of $\sim$10 nm wavelength are crucial for scalability of magnonics-based technologies [21,22], like signal transmission or memory-in-logic and logic-in-memory low-power digital computing architectures. However, they are difficult to excite by other methods due to the requirement for high magnetic fields [23,24].

The computational simulations of DW annihilation, [9,10,20] together with theoretical analysis of generic features of such a phenomenon [11], have been based *exclusively* on classical micromagnetics where one solves coupled Landau-Lifshitz-Gilbert (LLG) equations [25] for the dynamics of LMMs viewed as rotating classical vectors of fixed length. On the other hand, the dynamics of LMMs comprising two DWs also generates time-dependent fields which will push the surrounding conduction electrons out of equilibrium. The *nonequilibrium electrons* comprise pumped spin current [26–28] (as well as charge currents if the left-right symmetry of the device is broken [28,29]) in the absence of any externally applied bias voltage. The pumped spin currents flow out of the DW region into the external circuit, and since they carry away excess angular momentum of precessing LMMs, the *backaction* of nonequilibrium electrons on LMMs

*bnikolic@udel.edu

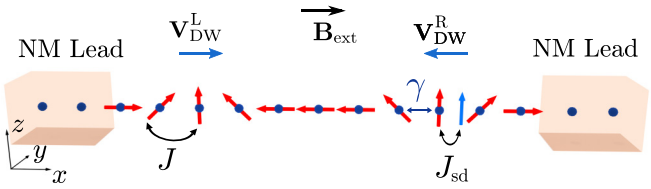

FIG. 1. Schematic view of a ferromagnetic nanowire modeled as a 1D tight-binding chain whose sites host classical LMMs (red arrows) interacting with spins (blue arrow) of conduction electrons. The nanowire is attached to two NM leads terminating into the macroscopic reservoirs kept at the *same* chemical potential. The two DWs within the nanowire carry opposite topological charge [8], $Q_L = -1$ for the L one and $Q_{\rm R} = +1$ for the R one. They collide with the opposite velocities $\mathbf{V}_{\rm DW}^L$ and $\mathbf{V}_{\rm DW}^R$ and annihilate, upon application of an external magnetic field $\mathbf{B}_{\rm ext}$ parallel to the nanowire, thereby mimicking the setup of the experiment in Ref. [20].

emerges [26] as an additional dampinglike (DL) spin-transfer torque (STT).

The STT, as a phenomenon in which spin angular momentum of conduction electrons is transferred to LMMs when they are not aligned with electronic spin-polarization, is usually discussed for *externally injected* spin current [30]. But here it is the result of a complicated many-body nonequilibrium state in which LMMs drive electrons out of equilibrium which, in turn, exert *backaction* in the form of STT onto LMMs to modify their dynamics in a self-consistent fashion [27,31]. Such effects are absent from classical micromagnetics or atomistic spin dynamics [25] because they do not include conduction electrons. This has prompted derivation of a multitude of phenomenological expressions [32–39] for the so-called *nonlocal* (i.e., magnetization-texture-dependent) and *spatially nonuniform* (i.e., position-dependent) Gilbert damping that could be added into the LLG equation and micromagnetics codes [40–42] to capture the *backaction* of nonequilibrium electrons while not simulating them explicitly. Such expressions do not require spin-orbit (SO) or magnetic disorder scattering, which are necessary for conventional local Gilbert damping [43–45], but they were estimated [33,36] to be usually a small effect unless additional conditions (such as narrow DWs or intrinsic SO coupling splitting the band structure [33]) are present. On the other hand, a *surprising* result [40] of Gilbert damping extracted from experiments on magnetic-field-driven DW being several times larger than the value obtained from standard ferromagnetic resonance measurements can only be accounted for by including additional nonlocal damping.

In this Letter, we unravel the complicated many-body nonequilibrium state of LMMs and conduction electrons created by DW annihilation using the recently developed [27,46–49] quantum-classical formalism which combines time-dependent nonequilibrium Green function (TDNEGF) [50,51] description of quantum dynamics of conduction electrons with the LLG equation description of classical dynamics of LMMs on each atom. [25] Such TDNEGF+LLG formalism is fully microscopic, since it requires only the quantum Hamiltonian of electrons and the classical Hamiltonian of LMMs as input, and is *numerically*

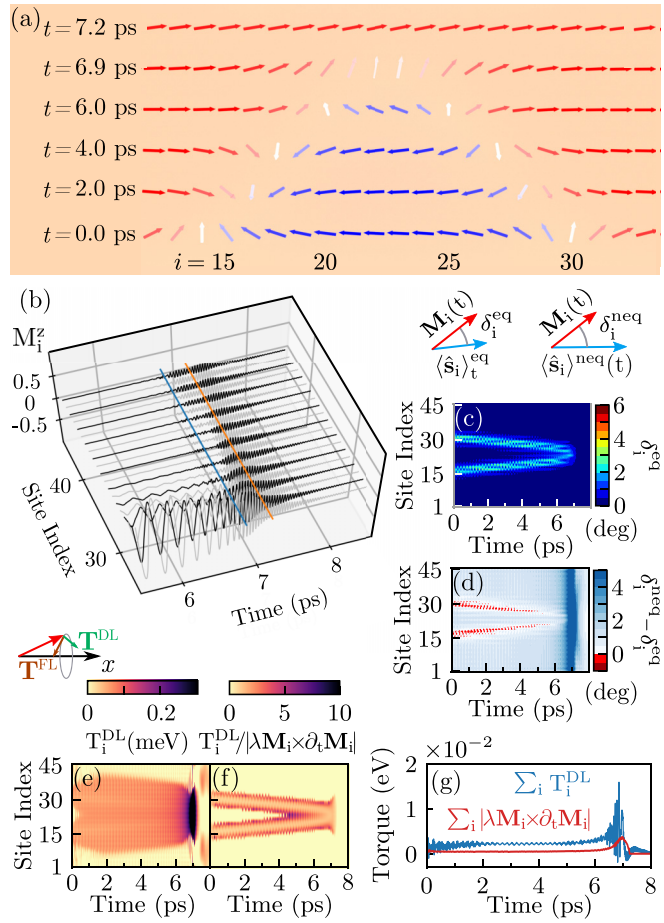

FIG. 2. (a) Sequence of snapshots of two DWs, in the course of their collision and annihilation in the setup of Fig. 1; and (b) the corresponding time dependence of the z component of LMMs where blue and orange lines mark $t = 6.9$ ps (when two DWs start vanishing) and $t = 7.2$ ps (when all LMMs become nearly parallel to the x axis) from panel (a). A movie animating panels (a) and (b) is provided in the Supplemental Material [58]. Spatiotemporal profile of: (c) angle $\delta_i^{\rm eq}$ and (d) "nonadiabaticity" angle $\delta_i^{\rm neq} - \delta_i^{\rm eq}$, with the meaning of $\delta_i^{\rm neq}$ and $\delta_i^{\rm eq}$ illustrated in the inset above panel (c); (e) DL STT [Eq. (3)] as electronic *backaction* on LMMs; (f) ratio of DL STT to conventional local Gilbert damping [Eq. (2)]; and (g) ratio of the sum of DL STT to the sum of conventional local Gilbert damping over all LMMs.

exact. We apply it to a setup depicted in Fig. 1 where two DWs reside at time $t = 0$ within a one-dimensional (1D) magnetic nanowire attached to two normal metal (NM) leads, terminating into the macroscopic reservoirs without any bias voltage.

Our *principal results* are: (i) annihilation of two DWs (Fig. 2) pumps highly unusual electronic spin currents whose power spectrum is *ultrabroadband* prior to the instant of annihilation [Fig. 3(d)], unlike the narrow peak around a single frequency for standard spin pumping [26]; (ii) because pumped spin currents carry away excess angular momentum of precessing LMMs, this acts as DL STT on LMMs which is spatially [Figs. 2(e) and 4(b)] and time [Fig. 2(g)] dependent, as well as $\simeq$2.4 times *larger* [Fig. 2(f)] than conventional local Gilbert damping [Eq. (2)]. This turns out to

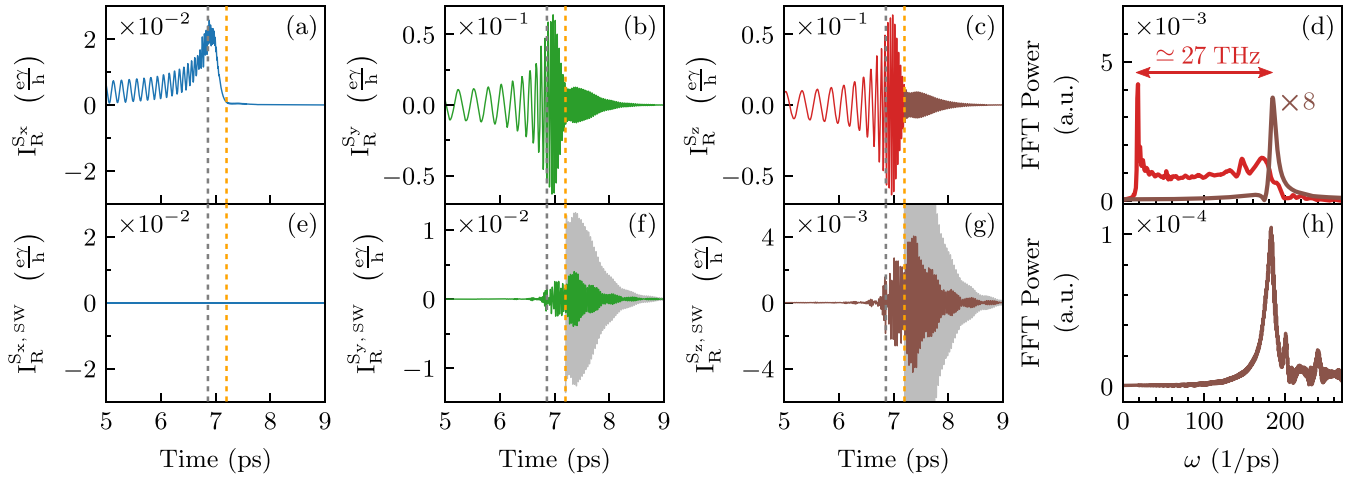

FIG. 3. Time dependence of: (a)–(c) electronic spin currents pumped into the right NM lead during DW collision and annihilation; (e)–(g) SW-generated contribution to spin currents in panels (a)–(c), respectively, after spin current carried by SW from Fig. 2(b) is stopped at the magnetic-nanowire/nonmagnetic-NM-lead interface and converted (as observed experimentally [20,61]) into electronic spin current in the right NM lead. Vertical dashed lines mark times $t = 6.9$ ps and $t = 7.2$ ps whose snapshots of LMMs are shown in Fig. 2(a). For easy comparison, gray curves in panels (f) and (g) are the same as the signal in panels (b) and (c), respectively, for postannihilation times $t \geqslant 7.2$ ps. Panels (d) and (h) plot FFT power spectrum of signals in panels (c) and (g), respectively, before (red curve) and after (brown curves) completed annihilation at $t = 7.2$ ps.

be *remarkably similar* to $\simeq$2.3 ratio of nonlocal and local Gilbert damping measured experimentally in permalloy, [40] but it is severely underestimated by phenomenological theories [32,33] [Figs. 4(a) and 4(b)].

Models and methods. The classical Hamiltonian for LMMs, described by unit vectors $\mathbf{M}_i(t)$ at each site i of 1D lattice, is chosen as

$$\mathcal{H} = -J\sum_{\langle ij\rangle}\mathbf{M}_i\cdot\mathbf{M}_j - K\sum_i\left(M_i^x\right)^2 + D\sum_i\left(M_i^y\right)^2 - \mu_B\sum_i\mathbf{M}_i\cdot\mathbf{B}_{\text{ext}}, \tag{1}$$

where $J = 0.1$ eV is the Heisenberg exchange coupling between the nearest-neighbor (as indicated by $\langle ij\rangle$) LMMs; $K = 0.05$ eV is the magnetic anisotropy along the x axis; and $D = 0.007$ eV is the demagnetizing field along the y axis. The last term in Eq. (1) is the Zeeman energy (μ_B is the Bohr magneton) describing the interaction of LMMs with an external magnetic field $\mathbf{B}_{\text{ext}}$ parallel to the nanowire in Fig. 1 driving the DW dynamics, as employed in the experiment [20]. The classical dynamics of LMMs is described by a system of coupled LLG equations [25] (using notation $\partial_t \equiv \partial/\partial t$)

$$\partial_t\mathbf{M}_i = -g\mathbf{M}_i\times\mathbf{B}_i^{\text{eff}} + \lambda\mathbf{M}_i\times\partial_t\mathbf{M}_i + \frac{g}{\mu_M}\left(\mathbf{T}_i\left[I_{\text{ext}}^{S_\alpha}\right] + \mathbf{T}_i[\mathbf{M}_i(t)]\right), \tag{2}$$

where $\mathbf{B}_i^{\text{eff}} = -\frac{1}{\mu_M}\partial\mathcal{H}/\partial\mathbf{M}_i$ is the effective magnetic field (μ_M is the magnitude of LMMs); g is the gyromagnetic ratio; and the magnitude of conventional local Gilbert damping is specified by spatially- and time-independent λ, set as $\lambda = 0.01$ as the typical value measured [40] in metallic ferromagnets. The spatial profile of a single DW in equilibrium, i.e., at time $t = 0$ as the initial condition, is given by $\mathbf{M}_i(Q, X_{\text{DW}}) = (\cos\phi_i(Q, X_{\text{DW}}),\ 0,\ \sin\phi_i(Q, X_{\text{DW}}))$, where $\phi_i(Q, X_{\text{DW}}) = Q\arccos[\tanh(x_i - X_{\text{DW}})]$; Q is the topological charge; and X_{DW} is the position of the DW. The initial configuration of two DWs, $\mathbf{M}_i(t=0) = \mathbf{M}_i(Q_{\text{L}}, X_{\text{L}}) + \mathbf{M}_i(Q_{\text{R}}, X_{\text{R}})$, positioned at sites $X_{\text{L}} = 15$ and $X_{\text{R}} = 30$ harbors opposite topological charges $Q_{\text{R}} = -Q_{\text{L}} = 1$ around these sites.

In general, two additional terms [32,33,52] in Eq. (2) extend the original LLG equation—STT due to externally

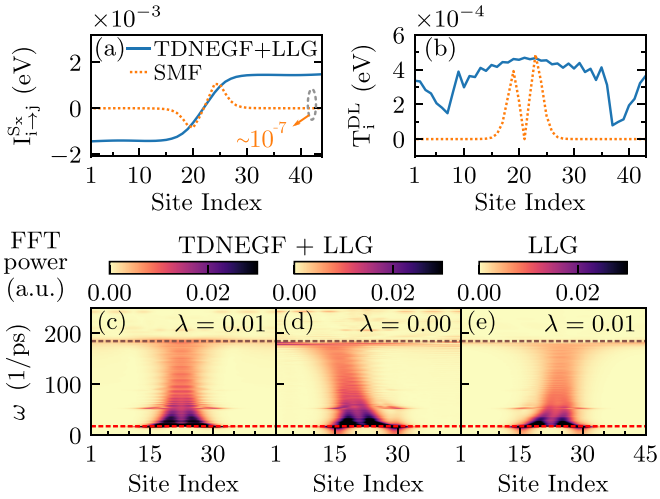

FIG. 4. Spatial profile at $t = 6.9$ ps of: (a) locally pumped spin current $I_{i\to j}^{S_x}$ [47] between sites i and j; and nonlocal damping due to *backaction of nonequilibrium electrons*. Solid lines in (a) and (b) are obtained from TDNEGF+LLG calculations, and dashed lines are obtained from SMF theory phenomenological formulas [32,33,69]. (c)–(e) FFT power spectra [22] of $M_i^z(t)$ where (c) and (d) are TDNEGF+LLG-computed with $\lambda = 0.01$ and $\lambda = 0$, respectively, while (e) is LLG-computed with *backaction* of nonequilibrium electrons removed, $\mathbf{T}_i[\mathbf{M}_i(t)] \equiv 0$, in Eq. (2). The dashed horizontal lines in panels (c)–(e) mark frequencies of peaks in Fig. 3(d).

injected electronic spin current [30], which is actually *absent* $\mathbf{T}_i[I^{S_\alpha}_{\rm ext}] \equiv 0$ in the setup of Fig. 1; and STT due to *backaction* of electrons

$$\mathbf{T}_i[\mathbf{M}_i(t)] = J_{\rm sd}\big(\langle\hat{\mathbf{s}}_i\rangle^{\rm neq}(t) - \langle\hat{\mathbf{s}}_i\rangle^{\rm eq}_t\big) \times \mathbf{M}_i(t), \tag{3}$$

driven out of equilibrium by $\mathbf{M}_i(t)$. Here $J_{\rm sd} = 0.1$ eV is chosen as the *s-d* exchange coupling (as measured in permalloy [53]) between LMMs and electron spin. We obtain "adiabatic" [54,55] electronic spin density, $\langle\hat{\mathbf{s}}_i\rangle^{\rm eq}_t = {\rm Tr}\,[\boldsymbol{\rho}^{\rm eq}_t|i\rangle\langle i| \otimes \boldsymbol{\sigma}]$, from grand canonical equilibrium density matrix (DM) for instantaneous configuration of $\mathbf{M}_i(t)$ at time t [see Eq. (5)]. Here $\boldsymbol{\sigma} = (\hat{\sigma}_x, \hat{\sigma}_y, \hat{\sigma}_z)$ is the vector of the Pauli matrices. The nonequilibrium electronic spin density, $\langle\hat{\mathbf{s}}_i\rangle^{\rm neq}(t) = {\rm Tr}\,[\boldsymbol{\rho}_{\rm neq}(t)|i\rangle\langle i| \otimes \boldsymbol{\sigma}]$, requires us to compute time-dependent nonequilibrium DM, $\boldsymbol{\rho}_{\rm neq}(t) = \hbar\mathbf{G}^<(t,t)/i$, which we construct using TDNEGF algorithms explained in Refs. [56,57] and combine [27] with the classical LLG equations [Eq. (2)] using time step $\delta t = 0.1$ fs. The TDNEGF calculations require as an input a quantum Hamiltonian for electrons, which is chosen as the tight-binding one

$$\hat{H}(t) = -\gamma \sum_{\langle ij\rangle} \hat{c}^\dagger_i \hat{c}_j - J_{\rm sd} \sum_i \hat{c}^\dagger_i \boldsymbol{\sigma} \cdot \mathbf{M}_i(t) \hat{c}_i. \tag{4}$$

Here $\hat{c}^\dagger_i = (\hat{c}^\dagger_{i\uparrow}, \hat{c}^\dagger_{i\downarrow})$ is a row vector containing operators $\hat{c}^\dagger_{i\sigma}$ which create an electron of spin $\sigma = \uparrow, \downarrow$ at the site i, and $\hat{c}_i$ is a column vector that contains the corresponding annihilation operators; and $\gamma = 1$ eV is the nearest-neighbor hopping. The magnetic nanowire in the setup in Fig. 1 consists of 45 sites and it is attached to semi-infinite NM leads modeled by the first term in $\hat{H}$. The Fermi energy of the reservoirs is set at $E_F = 0$ eV. Due to the computational complexity of TDNEGF calculations, [51] we use magnetic field $|\mathbf{B}_{\rm ext}| = 100$ T to complete DW annihilation on ∼ps time scale (in the experiment [20] this happens within ∼2 ns).

Results. Figure 2(a) demonstrates that TDNEGF+LLG-computed snapshots of $\mathbf{M}_i(t)$ *fully reproduce* annihilation in the experiment, [20] including *finale* when SW burst is emitted at $t \simeq 7.2$ ps in Fig. 2(b). The corresponding complete spatiotemporal profiles are animated as a movie provided in the Supplemental Material (SM). [58] However, in contrast to micromagnetic simulations of Ref. [20] where electrons are absent, Fig. 2(d) shows that they generate spin density $\langle\hat{\mathbf{s}}_i\rangle^{\rm neq}(t)$ which is *noncollinear* with either $\mathbf{M}_i(t)$ or $\langle\hat{\mathbf{s}}_i\rangle^{\rm eq}_t$. This leads to "nonadiabaticity" angle $(\delta^{\rm neq}_i - \delta^{\rm eq}_i) \neq 0$ in Fig. 2(d) and nonzero STT [Eq. (3) and Fig. 2(e)] as the self-consistent *backaction* of conduction electrons onto LMMs driven out of equilibrium by the dynamics of LMMs themselves. The STT vector, $\mathbf{T}_i = \mathbf{T}^{\rm FL}_i + \mathbf{T}^{\rm DL}_i$, can be decomposed [see inset above Fig. 2(e)] into (i) even under time-reversal or fieldlike torque, which affects precession of LMM around $\mathbf{B}^{\rm eff}_i$; and (ii) odd under time-reversal or DL torque, which either enhances the Gilbert term [Eq. (2)] by pushing LMM toward $\mathbf{B}^{\rm eff}_i$ or competes with it as antidamping. Figure 2(f) shows that $\mathbf{T}^{\rm DL}_i[\mathbf{M}_i(t)]$ acts like an additional nonlocal damping while being ≃2.4 times larger than conventional local Gilbert damping $\lambda\mathbf{M}_i \times \partial_t\mathbf{M}_i$ [Eq. (2)].

The quantum transport signature of DW vanishing within the time interval $t = 6.9$–7.2 ps in Fig. 2(a) is the reduction in the magnitude of pumped electronic spin currents [Figs. 3(a)–3(c)]. In fact, $I^{S_x}_{\rm R}(t) \to 0$ becomes zero [Fig. 3(a)] at $t = 7.2$ ps at which LMMs in Fig. 2(a) turn nearly parallel to the x axis while precessing around it. The frequency power spectrum [red curve in Fig. 3(d)] obtained from fast Fourier transform (FFT) of $I^{S_z}_{\rm R}(t)$, for times prior to completed annihilation and SW burst at $t = 7.2$ ps, reveals highly unusual spin pumping over an *ultrabroadband* frequency range. This can be contrasted with the usual spin pumping [26] whose power spectrum is just a peak around a single frequency [59], as also obtained [brown curve in Fig. 3(d)] by FFT of $I^{S_z}_{\rm R}(t)$ for postannihilation times $t > 7.2$ ps.

The spin current in Figs. 3(a)–3(c) has contributions from both electrons moved by time-dependent $\mathbf{M}_i(t)$ and SW hitting the magnetic-nanowire/NM-lead interface. At this interface, SW spin current is stopped and transmuted [47,48,60] into an electronic spin current flowing into the NM lead. The transmutation is often employed experimentally for direct electrical detection of SWs, where an electronic spin current on the NM side is converted into a voltage signal via the inverse spin Hall effect. [20,61] Within the TDNEGF+LLG picture, SW reaching the last LMM of the magnetic nanowire, at the sites $i = 1$ or $i = 45$ in our setup, initiates their dynamics whose coupling to conduction electrons in the neighboring left and right NM leads, respectively, leads to pumping [47] of the electronic spin current into the NM leads. The properly isolated electronic spin current due to transmutation of SW burst, which we denote by $I^{S_\alpha,{\rm SW}}_p$, is either zero or very small until the burst is generated in Figs. 3(e)–3(g), as expected. We note that detected spin current in the NM leads was attributed in the experiment [20] solely to SWs, which corresponds in our picture to considering only $I^{S_\alpha,{\rm SW}}_p$ while disregarding $I^{S_\alpha}_p - I^{S_\alpha,{\rm SW}}_p$.

Discussion. A computationally simpler alternative to our numerical self-consistent TDNEGF+LLG is to "integrate out electrons" [31,62–65] and derive effective expressions solely in terms of $\mathbf{M}_i(t)$, which can then be added into the LLG Eq. (2) and micromagnetics codes. [40–42] For example, spin motive force (SMF) theory [69] gives $I^{S_x}_{\rm SMF}(x) = \frac{g\mu_B\hbar G_0}{4e^2}[\partial\mathbf{M}(x,t)/\partial t \times \partial\mathbf{M}(x,t)/\partial x]_x$ for the spin current pumped by dynamical magnetic texture, so that $\mathbf{M} \times \mathcal{D} \cdot \partial_t\mathbf{M}$ is the corresponding nonlocal Gilbert damping [32,33]. Here $\mathbf{M}(x,t)$ is the local magnetization (assuming our 1D system); $\mathcal{D}_{\alpha\beta} = \eta\sum_\nu(\mathbf{M} \times \partial_\nu\mathbf{M})_\alpha(\mathbf{M} \times \partial_\nu\mathbf{M})_\beta$ (using notation $\alpha, \beta, \nu \in \{x, y, z\}$) is 3×3 spatially dependent damping tensor; and $\eta = \frac{g\mu_B\hbar G_0}{4e^2}$ with $G_0 = G^\uparrow + G^\downarrow$ being the total conductivity. We compare in Fig. 4: (i) spatial profile of $I^{S_x}_{\rm SMF}(x)$ to locally pumped spin current $I^{S_x}_{i\to j}$ [47] from TDNEGF+LLG calculations [Fig. 4(a)] to find that the former predicts negligible spin current flowing into the leads, thereby missing *ultrabroadband* spin pumping predicted in Fig. 3(d); (ii) spatial profile of $\mathbf{M} \times \mathcal{D} \cdot \partial_t\mathbf{M}$ to DL STT $T^{\rm DL}_i$ from TDNEGF+LLG calculations, to find that the former has comparable magnitude only within the DW region but with substantially differing profiles. Note also that [47] $[\sum_i \mathbf{T}_i(t)]_\alpha = \frac{\hbar}{2e}[I^{S_\alpha}_L(t) + I^{S_\alpha}_{\rm R}(t)] + \sum_i \frac{\hbar}{2}\frac{\partial\langle\hat{\mathbf{s}}^\alpha_i\rangle^{\rm neq}}{\partial t}$, which makes the sum of DL STT plotted in Fig. 2(g) time-dependent during collision,

in contrast to the sum of local Gilbert damping shown in Fig. 2(g). The *backaction of nonequilibrium electrons* via $\mathbf{T}_i[\mathbf{M}_i(t)]$ can strongly affect the dynamics of LMMs, especially for the case of short wavelength SWs and narrow DWs, [32,33,41,42] as confirmed by comparing FFT power spectra of $M_i^z(t)$ computed by TDNEGF+LLG [Figs. 4(c) and 4(d)] with those from LLG calculations [Fig. 4(e)] without any *backaction*.

We note that SMF theory [69] is derived in the "adiabatic" limit, [2,54] which assumes that electron spin remains in the the lowest energy state at each time. "Adiabaticity" is used in two different contexts in spintronics with noncollinear magnetic textures—temporal and spatial [2]. In the former case, such as when electrons interact with classical macrospin due to collinear LMMs, one assumes that classical spins are slow and $\langle\hat{\mathbf{s}}_i\rangle^{\rm neq}(t)$ can "perfectly lock" [2] to the direction $\mathbf{M}_i(t)$ of LMMs. In the latter case, such as for electrons traversing thick DW, one assumes that electron spin keeps the lowest energy state by rotating according to the orientation of $\mathbf{M}_i(t)$ at each spatial point, thereby evading reflection from the texture [2]. The concept of "adiabatic" limit is made a bit more quantitative by considering [2] the ratio of relevant energy scales, $J_{\rm sd}/\hbar\omega \gg 1$ or $J_{\rm sd}/\mu_B|\mathbf{B}_{\rm ext}| \gg 1$, in the former case; or combination of energy and spatial scales, $J_{\rm sd}d_{\rm DW}/\hbar v_F = J_{\rm sd}d_{\rm DW}/\gamma a \gg 1$, in the latter case (where v_F is the Fermi velocity, a is the lattice spacing and $d_{\rm DW}$ is the DW thickness). In our simulations, $J_{\rm sd}/\mu_B|\mathbf{B}_{\rm ext}| \approx 10$ and $J_{\rm sd}d_{\rm DW}/\gamma a \approx 1$ for $d_{\rm DW} \approx 10a$ in Fig. 2(a). Thus, it seems that fair comparison of our results to SMF theory requires us to substantially increase $J_{\rm sd}$. However, $J_{\rm sd} = 0.1$ eV (i.e., $\gamma/J_{\rm sd}/ \sim 10$, for typical $\gamma \sim 1$ eV which controls how fast is quantum dynamics of electrons) in our simulations is fixed by measured properties of permalloy [53].

Let us recall that rigorous definition of "adiabaticity" assumes that conduction electrons within a closed quantum system [54] at time t are in the ground state $|\Psi_0\rangle$ for the given configuration of LMMs $\mathbf{M}_i(t)$, $|\Psi(t)\rangle = |\Psi_0[\mathbf{M}_i(t)]\rangle$; or in an open system [55] their quantum state is specified by the grand canonical DM

$$\boldsymbol{\rho}_t^{\rm eq} = -\frac{1}{\pi}\int dE\, {\rm Im}\mathbf{G}_t^r f(E), \tag{5}$$

where the retarded GF, $\mathbf{G}_t^r = [E - \mathbf{H}[\mathbf{M}_i(t)] - \boldsymbol{\Sigma}_L - \boldsymbol{\Sigma}_{\rm R}]^{-1}$, and $\boldsymbol{\rho}_t^{\rm eq}$ depend parametrically [66–68] (or implicitly, so we put t in the subscript) on time via instantaneous configuration of $\mathbf{M}_i(t)$, thereby effectively assuming $\partial_t\mathbf{M}_i(t) = 0$. Here ${\rm Im}\mathbf{G}_t^r = (\mathbf{G}_t^r - [\mathbf{G}_t^r]^\dagger)/2i$; $\boldsymbol{\Sigma}_{L,R}$ are self-energies due to the leads; and $f(E)$ is the Fermi function. For example, the analysis of Ref. [69] assumes $\langle\hat{\mathbf{s}}_i\rangle^{\rm neq}(t) \parallel \langle\hat{\mathbf{s}}_i\rangle_t^{\rm eq}$ to reveal the origin of spin and charge pumping in SMF theory—nonzero angle $\delta_i^{\rm eq}$ between $\langle\hat{\mathbf{s}}_i\rangle_t^{\rm eq}$ and $\mathbf{M}_i(t)$ with the transverse component scaling $|\langle\hat{\mathbf{s}}_i\rangle_t^{\rm eq} \times \mathbf{M}_i(t)|/(\langle\hat{\mathbf{s}}_i\rangle_t^{\rm eq} \cdot \mathbf{M}_i(t)) \propto 1/J_{\rm sd}$ as the signature of "adiabatic" limit. Note that our $\delta_i^{\rm eq} \lesssim 4^\circ$ [Fig. 2(c)] in the region of two DWs (and $\delta_i^{\rm eq} \to 0$ elsewhere). Additional Figs. S1– S3 in the SM, [58] where we isolate two neighboring LMMs from the right DW in Fig. 1 and put them in steady precession with frequency ω for simplicity of analysis, demonstrate that entering such an "adiabatic" limit requires unrealistically large $J_{\rm sd} \gtrsim 2$ eV. Also, our exact [55] result (Figs. S1(b)–S3(b) in the SM [58]) shows $|\langle\hat{\mathbf{s}}_i\rangle_t^{\rm eq} \times \mathbf{M}_i(t)|/(\langle\hat{\mathbf{s}}_i\rangle_t^{\rm eq} \cdot \mathbf{M}_i(t)) \propto 1/J_{\rm sd}^2$ (instead of $\propto 1/J_{\rm sd}$ of Ref. [69]). Changing $\hbar\omega$, which, according to Fig. 3(c), is effectively increased by the dynamics of annihilation from $\hbar\omega \simeq 0.01$ eV, set initially by $\mathbf{B}_{\rm ext}$, toward $\hbar\omega \simeq 0.1$ eV, only modifies scaling of the transverse component of $\langle\hat{\mathbf{s}}_i\rangle^{\rm neq}(t)$ with $J_{\rm sd}$ (Figs. S1(a)–S3(a), S4(b) and S4(d) in the SM [58]). The nonadiabatic corrections [55,66–68] take into account $\partial_t\mathbf{M}_i(t) \neq 0$. We note that only in the limit $J_{\rm sd} \to \infty$, $(\langle\hat{\mathbf{s}}_i\rangle^{\rm neq}(t) - \langle\hat{\mathbf{s}}_i\rangle_t^{\rm eq}) \to 0$. Nevertheless, multiplication of these two limits within Eq. (3) yields nonzero geometric STT [54,55], as signified by $J_{\rm sd}$-independent STT (Figs. S1(c)–S3(c) in the SM [58]). Otherwise, the "nonadiabaticity" angle is always present $(\delta_i^{\rm neq} - \delta_i^{\rm eq}) \neq 0$ [Fig. 2(d)], even in the absence of spin relaxation due to magnetic impurities or SO coupling [70], and it can be directly related to additional spin and charge pumping [48,70] (see also Figs. S1(f)–S3(f) in the SM [58]).

Conclusions and outlook. The pumped spin current over *ultrabroadband* frequency range [Fig. 3(d)], as our central prediction, can be converted into a rapidly changing transient charge current via the inverse spin Hall effect. [71–73]. Such charge current will, in turn, emit electromagnetic radiation covering ~0.03–27 THz range (for $|\mathbf{B}_{\rm ext}| \sim 1$ T) or ~0.3–27.3 THz range (for $|\mathbf{B}_{\rm ext}| \sim 10$ T), which is the highly sought range of frequencies for a variety of applications. [72,73].

Acknowledgments. M.D.P., U.B., and B.K.N. were supported by the US National Science Foundation (NSF) Grant No. ECCS 1922689. P.P. was supported by the US Army Research Office (ARO) MURI Award No. W911NF-14-1-0247.

[1] G. Tatara, H. Kohno, and J. Shibata, Microscopic approach to current-driven domain wall dynamics, Phys. Rep. **468**, 213 (2008).

[2] G. Tatara, Effective gauge field theory of spintronics, Physica E **106**, 208 (2019).

[3] K.-J. Kim, Y. Yoshimura, and T. Ono, Current-driven magnetic domain wall motion and its real-time detection, Jpn. J. Appl. Phys. **56**, 0802A4 (2017).

[4] S. Parkin and S.-H. Yang, Memory on the racetrack, Nat. Nanotech. **10**, 195 (2015).

[5] D. A. Allwood, G. Xiong, M. D. Cooke, C. C. Faulkner, D. Atkinson, N. Vernier, and R. P. Cowburn, Submicrometer ferromagnetic not gate and shift register, Science **296**, 2003 (2002).

[6] J. Grollier, D. Querlioz, and M. D. Stiles, Spintronic nanodevices for bioinspired computing, Proc. IEEE **104**, 2024 (2016).

[7] L. Thomas, M. Hayashi, R. Moriya, C. Rettner, and S. Parkin, Topological repulsion between domain walls in magnetic nanowires leading to the formation of bound states, Nat. Commun. **3**, 810 (2012).

[8] H.-B. Braun, Topological effects in nanomagnetism: From superparamagnetism to chiral quantum solitons, Adv. Phys. **61**, 1 (2012).

[9] A. Kunz, Field induced domain wall collisions in thin magnetic nanowires, Appl. Phys. Lett. **94**, 132502 (2009).

[10] A. Kunz and E. W. Rentsch, Simulations of field driven domain wall interactions in ferromagnetic nanowires, IEEE Trans. Magn. **46**, 1556 (2010).

[11] A. Ghosh, K. S. Huang, and O. Tchernyshyov, Annihilation of domain walls in a ferromagnetic wire, Phys. Rev. B **95**, 180408(R) (2017).

[12] S. K. Kim, S. Takei, and Y. Tserkovnyak, Topological spin transport by Brownian diffusion of domain walls, Phys. Rev. B **92**, 220409(R) (2015).

[13] N. Manton and P. Sutcliffe, *Topological Solitons* (Cambridge University Press, Cambridge, 2004).

[14] D. I. Bradley, S. N. Fisher, A. M. Guénault, R. P. Haley, J. Kopu, H. Martin, G. R. Pickett, J. E. Roberts, and V. Tsepelin, Relic topological defects from brane annihilation simulated in superfluid ^{3}He, Nat. Phys. **4**, 46 (2008).

[15] K. Nakayama, F. Takahashi, and N. Yokozaki, Gravitational waves from domain walls and their implications, Phys. Lett. B **770**, 500 (2017).

[16] G. Dvali and A. Vilenkin, Solitonic D-branes and brane annihilation, Phys. Rev. D **67**, 046002 (2003).

[17] Y. Shen and I. Dierking, Annihilation dynamics of topological defects induced by microparticles in nematic liquid crystals, Soft Matter **15**, 8749 (2019).

[18] H. Takeuchi, K. Kasamatsu, M. Tsubota, and M. Nitta, Tachyon Condensation Due to Domain-Wall Annihilation in Bose-Einstein Condensates, Phys. Rev. Lett. **109**, 245301 (2012).

[19] M. Nitta, K. Kasamatsu, M. Tsubota, and H. Takeuchi, Creating vortons and three-dimensional skyrmions from domain-wall annihilation with stretched vortices in Bose-Einstein condensates, Phys. Rev. A **85**, 053639 (2012).

[20] S. Woo, T. Delaney, and G. S. D. Beach, Magnetic domain wall depinning assisted by spin wave bursts, Nat. Phys. **13**, 448 (2017).

[21] A. V. Chumak, V. I. Vasyuchka, A. A. Serga, and B. Hillebrands, Magnon spintronics, Nat. Phys. **11**, 453 (2015).

[22] S.-K. Kim, Micromagnetic computer simulations of spin waves in nanometre-scale patterned magnetic elements, J. Phys. D: Appl. Phys **43**, 264004 (2010).

[23] A. Navabi *et al.*, Efficient Excitation of High-Frequency Exchange-Dominated Spin Waves in Periodic Ferromagnetic Structures, Phys. Rev. Appl. **7**, 034027 (2017).

[24] C. Liu *et al.*, Long-distance propagation of short-wavelength spin waves, Nat. Commun. **9**, 738 (2018).

[25] R. F. L. Evans, W. J. Fan, P. Chureemart, T. A. Ostler, M. O. A. Ellis, and R. W. Chantrell, Atomistic spin model simulations of magnetic nanomaterials, J. Phys.: Condens. Matter **26**, 103202 (2014).

[26] Y. Tserkovnyak, A. Brataas, G. E. W. Bauer, and B. I. Halperin, Nonlocal magnetization dynamics in ferromagnetic heterostructures, Rev. Mod. Phys. **77**, 1375 (2005).

[27] M. D. Petrović, B. S. Popescu, U. Bajpai, P. Plecháč, and B. K. Nikolić, Spin and Charge Pumping by a Steady or Pulse-Current-Driven Magnetic Domain Wall: A Self-Consistent Multiscale Time-Dependent Quantum-Classical Hybrid Approach, Phys. Rev. Appl. **10**, 054038 (2018).

[28] S.-H. Chen, C.-R. Chang, J. Q. Xiao, and B. K. Nikolić, Spin and charge pumping in magnetic tunnel junctions with precessing magnetization: A nonequilibrium Green function approach, Phys. Rev. B **79**, 054424 (2009).

[29] U. Bajpai, B. S. Popescu, P. Plecháč, B. K. Nikolić, L. E. F. Foa Torres, H. Ishizuka, and N. Nagaosa, Spatio-temporal dynamics of shift current quantum pumping by femtosecond light pulse, J. Phys.: Mater. **2**, 025004 (2019).

[30] D. Ralph and M. Stiles, Spin transfer torques, J. Magn. Mater. **320**, 1190 (2008).

[31] M. Sayad and M. Potthoff, Spin dynamics and relaxation in the classical-spin Kondo-impurity model beyond the Landau-Lifschitz-Gilbert equation, New J. Phys. **17**, 113058 (2015).

[32] S. Zhang and S. S.-L. Zhang, Generalization of the Landau-Lifshitz-Gilbert Equation for Conducting Ferromagnets, Phys. Rev. Lett. **102**, 086601 (2009).

[33] K.-W. Kim, J.-H. Moon, K.-J. Lee, and H.-W. Lee, Prediction of Giant Spin Motive Force Due to Rashba Spin-Orbit Coupling, Phys. Rev. Lett. **108**, 217202 (2012).

[34] J. Foros, A. Brataas, Y. Tserkovnyak, and G. E. W. Bauer, Current-induced noise and damping in nonuniform ferromagnets, Phys. Rev. B **78**, 140402(R) (2008).

[35] Y. Tserkovnyak, E. M. Hankiewicz, and G. Vignale, Transverse spin diffusion in ferromagnets, Phys. Rev. B **79**, 094415 (2009).

[36] E. M. Hankiewicz, G. Vignale, and Y. Tserkovnyak, Inhomogeneous Gilbert damping from impurities and electron-electron interactions, Phys. Rev. B **78**, 020404(R) (2008).

[37] Z. Yuan, K. M. D. Hals, Y. Liu, A. A. Starikov, A. Brataas, and P. J. Kelly, Gilbert Damping in Noncollinear Ferromagnets, Phys. Rev. Lett. **113**, 266603 (2014).

[38] H. Y. Yuan, Z. Yuan, K. Xia, and X. R. Wang, Influence of nonlocal damping on the field-driven domain wall motion, Phys. Rev. B **94**, 064415 (2016).

[39] D. Thonig, Y. Kvashnin, O. Eriksson, and M. Pereiro, Nonlocal Gilbert damping tensor within the torque-torque correlation model, Phys. Rev. Mater. **2**, 013801 (2018).

[40] T. Weindler, H. G. Bauer, R. Islinger, B. Boehm, J.-Y. Chauleau, and C. H. Back, Magnetic Damping: Domain Wall Dynamics Versus Local Ferromagnetic Resonance, Phys. Rev. Lett. **113**, 237204 (2014).

[41] W. Wang, M. Dvornik, M.-A. Bisotti, D. Chernyshenko, M. Beg, M. Albert, A. Vansteenkiste, B. V. Waeyenberge, A. N. Kuchko, V. V. Kruglyak, and H. Fangohr, Phenomenological description of the nonlocal magnetization relaxation in magnonics, spintronics, and domain-wall dynamics, Phys. Rev. B **92**, 054430 (2015).

[42] R. Verba, V. Tiberkevich, and A. Slavin, Damping of linear spin-wave modes in magnetic nanostructures: Local, nonlocal, and coordinate-dependent damping, Phys. Rev. B **98**, 104408 (2018).

[43] V. Kamberský, Spin-orbital Gilbert damping in common magnetic metals, Phys. Rev. B **76**, 134416 (2007).

[44] K. Gilmore, Y. U. Idzerda, and M. D. Stiles, Identification of the Dominant Precession-Damping Mechanism in Fe, Co, and Ni by First-Principles Calculations, Phys. Rev. Lett. **99**, 027204 (2007).

[45] A. A. Starikov, P. J. Kelly, A. Brataas, Y. Tserkovnyak, and G. E. W. Bauer, Unified First-Principles Study of Gilbert

Damping, Spin-Flip Diffusion, and Resistivity in Transition Metal Alloys, Phys. Rev. Lett. **105**, 236601 (2010).

[46] U. Bajpai and B. K. Nikolić, Time-retarded damping and magnetic inertia in the Landau-Lifshitz-Gilbert equation self-consistently coupled to electronic time-dependent nonequilibrium Green functions, Phys. Rev. B **99**, 134409 (2019).

[47] A. Suresh, M. D. Petrović, U. Bajpai, H. Yang, and B. K. Nikolić, Magnon- Versus Electron-Mediated Spin-Transfer Torque Exerted by Spin Current Across an Antiferromagnetic Insulator to Switch the Magnetization of an Adjacent Ferromagnetic Metal, Phys. Rev. Appl. **15**, 034089 (2021).

[48] A. Suresh, U. Bajpai, and B. K. Nikolić, Magnon-driven chiral charge and spin pumping and electron-magnon scattering from time-dependent quantum transport combined with classical atomistic spin dynamics, Phys. Rev. B **101**, 214412 (2020)

[49] E. V. Boström and C. Verdozzi, Steering magnetic skyrmions with currents: A nonequilibrium Green's functions approach, Phys. Stat. Solidi B **256**, 1800590 (2019).

[50] G. Stefanucci and R. van Leeuwen, *Nonequilibrium Many-Body Theory of Quantum Systems: A Modern Introduction* (Cambridge University Press, Cambridge, 2013).

[51] B. Gaury, J. Weston, M. Santin, M. Houzet, C. Groth, and X. Waintal, Numerical simulations of time-resolved quantum electronics, Phys. Rep. **534**, 1 (2014).

[52] S. Zhang and Z. Li, Roles of Nonequilibrium Conduction Electrons on the Magnetization Dynamics of Ferromagnets, Phys. Rev. Lett. **93**, 127204 (2004).

[53] R. L. Cooper and E. A. Uehling, Ferromagnetic resonance and spin diffusion in supermalloy, Phys. Rev. **164**, 662 (1967).

[54] C. Stahl and M. Potthoff, Anomalous Spin Precession Under a Geometrical Torque, Phys. Rev. Lett. **119**, 227203 (2017).

[55] U. Bajpai and B. K. Nikolić, Spintronics Meets Nonadiabatic Molecular Dynamics: Geometric Spin Torque and Damping on Dynamical Classical Magnetic Texture Due to an Electronic Open Quantum System, Phys. Rev. Lett. **125**, 187202 (2020).

[56] A. Croy and U. Saalmann, Propagation scheme for nonequilibrium dynamics of electron transport in nanoscale devices, Phys. Rev. B **80**, 245311 (2009).

[57] B. S. Popescu and A. Croy, Efficient auxiliary-mode approach for time-dependent nanoelectronics, New J. Phys. **18**, 093044 (2016).

[58] See Supplemental Material at http://link.aps.org/supplemental/10.1103/PhysRevB.104.L020407 for (i) a movie animating classical LMMs in Figs. 2(a) and 2(b); and (ii) four additional figures showing orientation of nonequilibrium and "adiabatic" electronic spin density with respect to LMMs as a function of J_{sd} for a simplified system (amenable to analytically exact treatment [55]) of two LMMs isolated from the right DW in Fig. 1 and put into steady precession with a constant frequency ω (we use three different values for ω as parameter, and we also show how these orientations change with increasing the thickness d_{DW} of the DW from which two LMMs are isolated).

[59] L. Bocklage, Coherent THz Transient Spin Currents by Spin Pumping, Phys. Rev. Lett. **118**, 257202 (2017).

[60] G. E. Bauer and Y. Tserkovnyak, Viewpoint: Spin-magnon transmutation, Physics **4**, 40 (2011).

[61] A. V. Chumak, A. A. Serga, M. B. Jungfleisch, R. Neb, D. A. Bozhko, V. S. Tiberkevich, and B. Hillebrands, Direct detection of magnon spin transport by the inverse spin Hall effect, Appl. Phys. Lett. **100**, 082405 (2012).

[62] M. Onoda and N. Nagaosa, Dynamics of Localized Spins Coupled to the Conduction Electrons with Charge and Spin Currents, Phys. Rev. Lett. **96**, 066603 (2006).

[63] A. S. Núñez and R. A. Duine, Effective temperature and Gilbert damping of a current-driven localized spin, Phys. Rev. B **77**, 054401 (2008).

[64] J. Fransson and J.-X. Zhu, Spin dynamics in a tunnel junction between ferromagnets, New J. Phys. **10**, 013017 (2008).

[65] H. M. Hurst, V. Galitski, and T. T. Heikkilä, Electron-induced massive dynamics of magnetic domain walls, Phys. Rev. B **101**, 054407 (2020).

[66] N. Bode, S. V. Kusminskiy, R. Egger, and F. von Oppen, Scattering Theory of Current-Induced Forces in Mesoscopic Systems, Phys. Rev. Lett. **107**, 036804 (2011).

[67] M. Thomas, T. Karzig, S. V. Kusminskiy, G. Zaránd, and F. von Oppen, Scattering theory of adiabatic reaction forces due to out-of-equilibrium quantum environments, Phys. Rev. B **86**, 195419 (2012).

[68] F. Mahfouzi, B. K. Nikolić, and N. Kioussis, Antidamping spin-orbit torque driven by spin-flip reflection mechanism on the surface of a topological insulator: A time-dependent nonequilibrium Green function approach, Phys. Rev. B **93**, 115419 (2016).

[69] Y. Yamane, J. Ieda, J.-I. Ohe, S. E. Barnes, and S. Maekawa, Equation-of-motion approach of spin-motive force, J. Appl. Phys. **109**, 07C735 (2011).

[70] M. Evelt, H. Ochoa, O. Dzyapko, V. E. Demidov, A. Yurgens, J. Sun, Y. Tserkovnyak, V. Bessonov, A. B. Rinkevich, and S. O. Demokritov, Chiral charge pumping in graphene deposited on a magnetic insulator, Phys. Rev. B **95**, 024408 (2017).

[71] D. Wei, M. Obstbaum, M. Ribow, C. H. Back, and G. Woltersdorf, Spin Hall voltages from a.c. and d.c. spin currents, Nat. Commun. **5**, 3768 (2014).

[72] T. Seifert *et al.*, Efficient metallic spintronic emitters of ultra-broadband terahertz radiation, Nat. Photon. **10**, 483 (2016).

[73] M. Chen, Y. Wu, Y. Liu, K. Lee, X. Qiu, P. He, J. Yu, and H. Yang, Current-enhanced broadband THz emission from spintronic devices, Adv. Opt. Mater. **7**, 1801608 (2019).

Supplemental Material for "Annihilation of topological solitons in magnetism with spin wave burst finale: The role of nonequilibrium electrons causing nonlocal damping and spin pumping over ultrabroadband frequency range"

Marko D. Petrović,[1] Utkarsh Bajpai,[1] Petr Plecháč,[2] and Branislav K. Nikolić[1,*]

[1] *Department of Physics and Astronomy, University of Delaware, Newark, DE 19716, USA*
[2] *Department of Mathematical Sciences, University of Delaware, Newark, DE 19716, USA*

In addition to a movie animating Fig. 2 in the main text, Supplemental Material provides four additional figures. Figures S1–S3 show orientation of electronic nonequilibrium $\langle \hat{\mathbf{s}}_i \rangle^{\rm neq}(t)$ and "adiabatic" $\langle \hat{\mathbf{s}}_i \rangle_t^{\rm eq}$ spin densities (defined in the main text) with respect to two classical localized magnetic moments (LMM). The two LMMs are isolated [top inset of Fig. S4] as the neighboring ones from the right magnetic domain wall (DW) in Fig. 1 in the main text. For simplicity of analysis, and in order to be able to employ the *exact* time-dependent nonequilibrium density matrix derived in Ref. [1], we assume that LMMs are steadily precessing with frequency ω, as illustrated in the inset on the top of each Figs. S1–S3. Their dynamics then drives conduction electrons within an infinite one-dimensional tight-binding chain out of equilibrium, thereby generating $\langle \hat{\mathbf{s}}_i \rangle^{\rm neq}(t)$ and $\langle \hat{\mathbf{s}}_i \rangle_t^{\rm eq}$. This setup makes it possible to obtain *exact* scaling of $\langle \hat{\mathbf{s}}_i \rangle^{\rm neq}(t)$, $\langle \hat{\mathbf{s}}_i \rangle_t^{\rm eq}$, spin-transfer torque due to *backaction of nonequilibrium electrons* [Eq. (3) in the main text and panel (c) in Figs. S1–S3] and total spin current pumped into the leads [panel (f) in Figs. S1–S3] with the strength $J_{\rm sd}$ [Eq. (4) in the main text] of *sd* exchange interaction between conduction electron spin and classical LMMs.

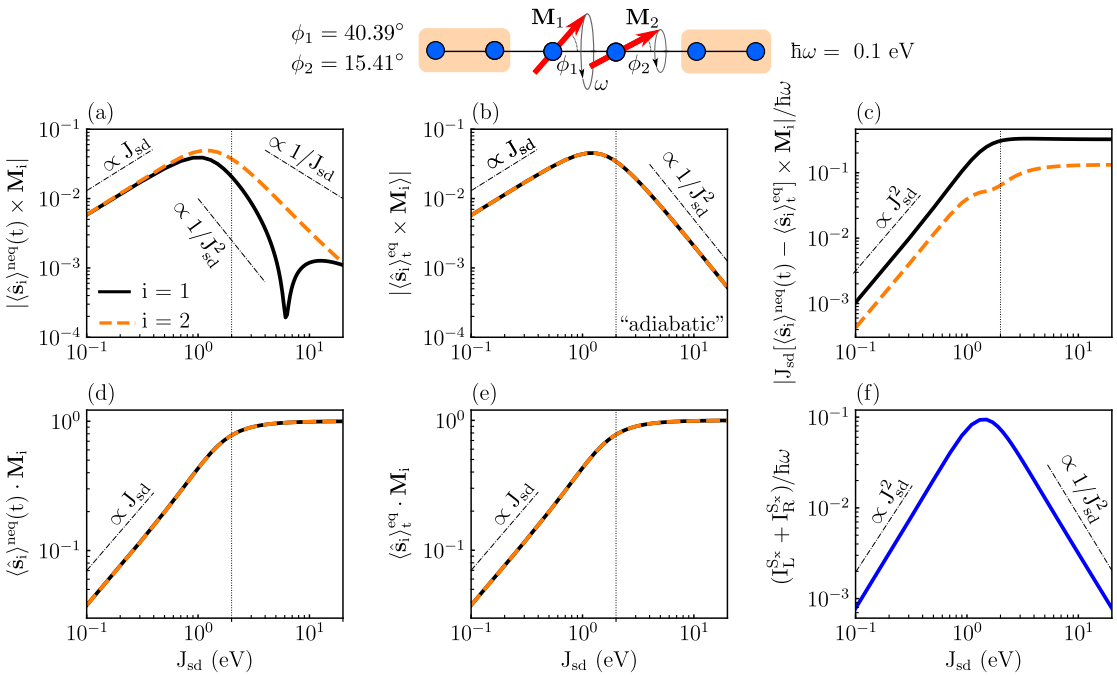

FIG. S1. The dependence on $J_{\rm sd}$ of: (a) transverse component, with respect to $\mathbf{M}_i(t)$, of nonequilibrium electronic spin density $\langle \hat{\mathbf{s}}_i \rangle^{\rm neq}(t)$; (d) longitudinal component of $\langle \hat{\mathbf{s}}_i \rangle^{\rm neq}(t)$; (b) transverse component of "adiabatic" electronic spin density $\langle \hat{\mathbf{s}}_i \rangle_t^{\rm eq}$; (d) longitudinal component of $\langle \hat{\mathbf{s}}_i \rangle_t^{\rm eq}$; (c) modulus of spin-transfer torque [Eq. (3) in the main text] as *backaction of nonequilibrium electrons* onto LMMs. (f) The z-component (the x-axis is along the chain in the inset on the top) of the total electronic spin current, $I_L^{S_z} + I_R^{S_z}$ pumped into the left (L) and right (R) leads. The frequency of precession of two LMMs is $\hbar\omega = 0.1$ eV and electronic hopping (between the tight-binding sites in the inset on the top) is $\gamma = 1$ eV. The interval $J_{\rm sd}/\gamma \gtrsim 2.0$, where the transverse components of $\langle \hat{\mathbf{s}}_i \rangle^{\rm neq}(t)$ and $\langle \hat{\mathbf{s}}_i \rangle_t^{\rm eq}$ start to decay [2] with $J_{\rm sd}$ [panels (a) and (b)], while the corresponding STT on LMMs due to backaction of nonequilibrium electrons [panel (c)] is constant [1], is marked as "adiabatic" [2].

* bnikolic@udel.edu

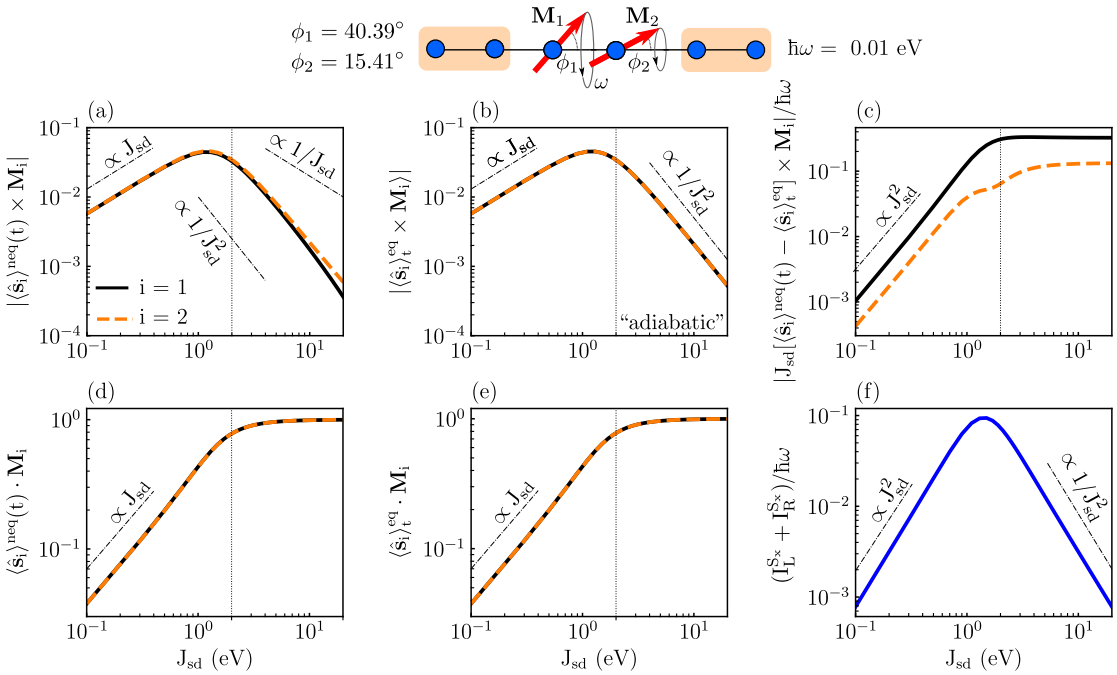

FIG. S2. Same information as in Fig. S1 but for the frequency of precession $\hbar\omega = 0.01$ eV of two LMMs in the top inset.

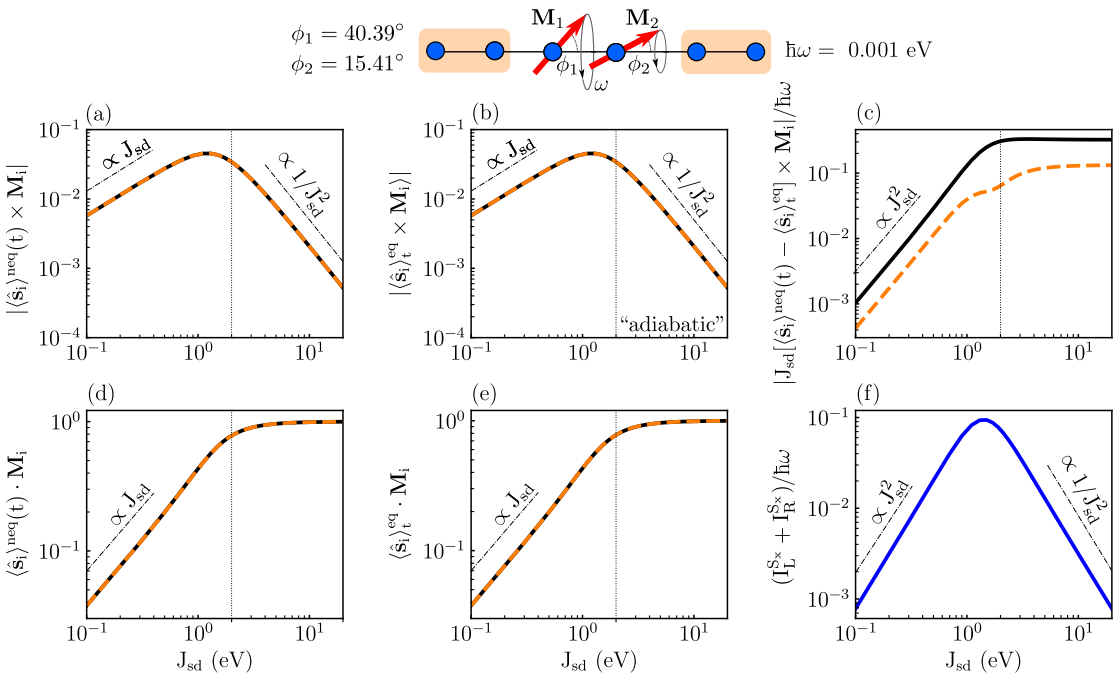

FIG. S3. Same information as in Fig. S1 but for the frequency of precession $\hbar\omega = 0.001$ eV of two LMMs in the top inset.

To further clarify the scaling of $|\langle \hat{\mathbf{s}}_i\rangle^{\rm neq}(t) \times \mathbf{M}_i(t)|$ with $J_{\rm sd}$ in Figs. S1–S3, let us consider

$$\langle \hat{\mathbf{s}}_i\rangle^{\rm neq}(t) = \langle \hat{\mathbf{s}}_i\rangle_t^{\rm eq} + \left[\langle \hat{\mathbf{s}}_i\rangle^{\rm neq}(t) - \langle \hat{\mathbf{s}}_i\rangle_t^{\rm eq}\right], \tag{1}$$

whose cross-product with $\mathbf{M}_i(t)$ furnishes

$$\langle \hat{\mathbf{s}}_i\rangle^{\rm neq}(t) \times \mathbf{M}_i = \langle \hat{\mathbf{s}}_i\rangle_t^{\rm eq} \times \mathbf{M}_i + \left[\langle \hat{\mathbf{s}}_i\rangle^{\rm neq}(t) - \langle \hat{\mathbf{s}}_i\rangle_t^{\rm eq}\right] \times \mathbf{M}_i. \tag{2}$$

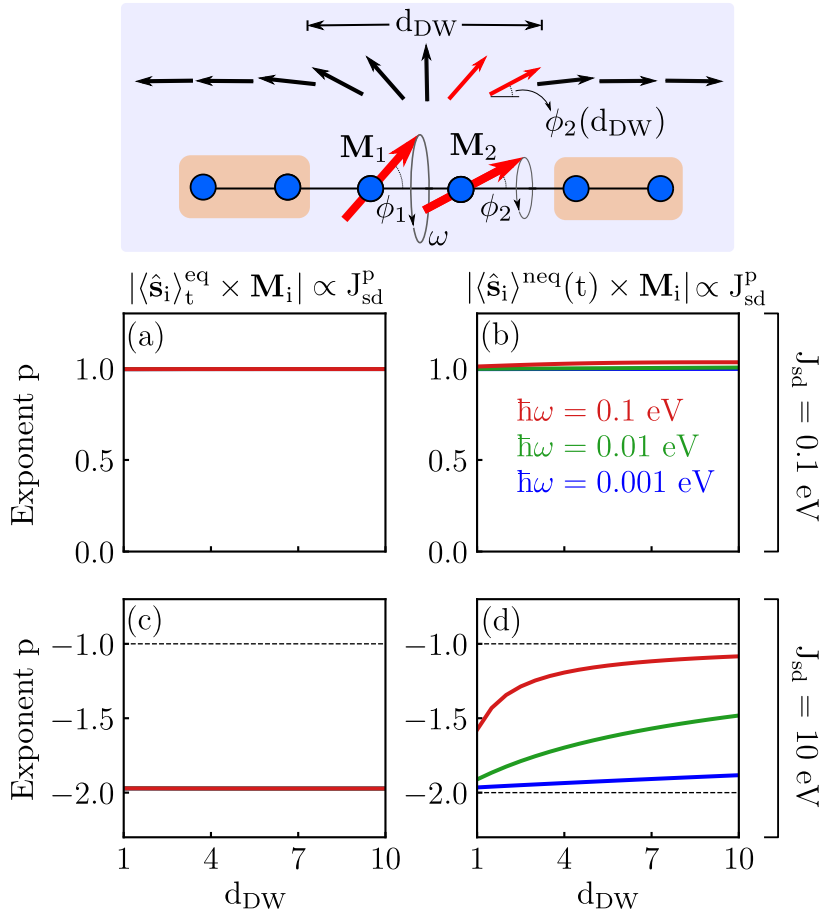

FIG. S4. The dependence of $|\langle\hat{\mathbf{s}}_i\rangle_t^{\rm eq}\times\mathbf{M}_i(t)|$ and $|\langle\hat{\mathbf{s}}_i\rangle^{\rm neq}(t)\times\mathbf{M}_i(t)|$ from Figs. S1–S3 on the thickness $d_{\rm DW}$ (denoted in the top inset) of a magnetic DW from which two precessing LMMs (red arrows in the top inset) are isolated. We use two different values $J_{\rm sd}=0.1$ eV [panels (a) and (b)] or $J_{\rm sd}=10.0$ eV [panels (c) and (d)] as parameters for which electron spin dynamics is nonadiabatic or "adiabatic" in Figs. S1–S3, respectively.

Within the "adiabatic" regime labeled in panel (b) of Figs. S1–S3, we find

$$|\langle\hat{\mathbf{s}}_i\rangle_t^{\rm eq}\times\mathbf{M}_i|=\frac{\mathcal{A}_i^{\rm eq}(t)}{J_{\rm sd}^2}, \tag{3}$$

where $\mathcal{A}_i^{\rm eq}(t)$ is a constant of proportionality. Similarly, from the "adiabatic" regime in panel (c) of Figs. S1–S3, we deduce

$$\left|\left[\langle\hat{\mathbf{s}}_i\rangle^{\rm neq}(t)-\langle\hat{\mathbf{s}}_i\rangle_t^{\rm eq}\right]\times\mathbf{M}_i\right|=\frac{\hbar\omega}{J_{\rm sd}}\mathcal{A}_i(t), \tag{4}$$

where $\mathcal{A}_i(t)$ is a constant of proportionality that encodes *purely nonequilibrium* properties. By using Eqs. (3) and (4) in the modulus of Eq. (2) we obtain

$$\left|\langle\hat{\mathbf{s}}_i\rangle^{\rm neq}(t)\times\mathbf{M}_i\right|=\left\{\left[\frac{\mathcal{A}_i^{\rm eq}(t)}{J_{\rm sd}^2}\right]^2+\left[\frac{\hbar\omega}{J_{\rm sd}}\mathcal{A}_i(t)\right]^2+2\left[\frac{\mathcal{A}_i^{\rm eq}(t)}{J_{\rm sd}^2}\right]\left[\frac{\hbar\omega}{J_{\rm sd}}\mathcal{A}_i(t)\right]\cos\theta_i(t)\right\}^{1/2}, \tag{5}$$

where $\theta_i(t)$ is the angle between the vectors $\langle\hat{\mathbf{s}}_i\rangle_t^{\rm eq}\times\mathbf{M}_i$ and $[\langle\hat{\mathbf{s}}_i\rangle^{\rm neq}(t)-\langle\hat{\mathbf{s}}_i\rangle_t^{\rm eq}]\times\mathbf{M}_i$. Retaining only those terms that are linear in $\hbar\omega$ in Eq. (5) yields

$$|\langle\hat{\mathbf{s}}_i\rangle^{\rm neq}(t)\times\mathbf{M}_i|=\frac{\mathcal{A}_i^{\rm eq}(t)}{J_{\rm sd}^2}+\frac{\hbar\omega}{J_{\rm sd}}\mathcal{A}_i(t)\cos\theta_i(t). \tag{6}$$

Equation (6) shows that in the "adiabatic" regime, the transverse component [with respect to $\mathbf{M}_i$] of nonequilibrium spin density $\langle \hat{\mathbf{s}}_i \rangle^{\rm neq}(t)$, depends on nontrivial combination of two terms that are proportional to $1/J_{\rm sd}^2$ and $\hbar\omega/J_{\rm sd}$. Such dependence is confirmed by Fig. S1(a) where $\hbar\omega = 0.1$ eV. Reducing the frequency of precession ω, such as $\hbar\omega = 0.01$ eV [Fig. S2] and $\hbar\omega = 0.001$ eV [Fig. S3], reveals that the second term in Eq. (6) progressively looses its importance and the first term prevails leading eventually to $|\langle \hat{\mathbf{s}}_i \rangle^{\rm neq}(t) \times \mathbf{M}_i| \propto 1/J_{\rm sd}^2$.

The size of noncollinear magnetic texture, such as $d_{\rm DW}$ as the thickness of DW denoted in the top inset of Fig. S4, affects "spatial adiabaticity" [3] and, therefore, it can modify scaling $|\langle \hat{\mathbf{s}}_i \rangle^{\rm neq}(t) \times \mathbf{M}_i| \propto J_{\rm sd}^p$. On the other hand, $d_{\rm DW}$ does not affect scaling of $\langle \hat{\mathbf{s}}_i \rangle_t^{\rm eq}$ in Figs. S4(a) and S4(c). We extract exponent p in Fig. S4(b) for $J_{\rm sd} = 0.1$ eV (as used in the main text) to find $p \approx 1$ that is largely independent of $d_{\rm DW}$. However, once the "adiabatic" regime from Figs. S1–S3 is entered by choosing $J_{\rm sd} = 10$ eV, Fig. S4(d) shows how exponent p becomes sensitive to the value of $d_{\rm DW}$. The stronger dependence on $d_{\rm DW}$ is found for larger values of $\hbar\omega$, while revealing that the exponent reaches $p \to -1$ asymptotically with increasing $d_{\rm DW}$. This can interpreted using Eq. (6) where for larger values of $d_{\rm DW}$ the first term progressively looses its importance and the second term prevails, leading eventually to $|\langle \hat{\mathbf{s}}_i \rangle^{\rm neq}(t) \times \mathbf{M}_i| \propto 1/J_{\rm sd}$ in Fig. S4(d).

[1] U. Bajpai and B. K. Nikolić, Spintronics meets nonadiabatic molecular dynamics: Geometric spin torque and damping on dynamical classical magnetic texture due to an electronic open quantum system, Phys. Rev. Lett. **125**, 187202 (2020).

[2] Y. Yamane, J. Ieda, J.-I. Ohe, S. E. Barnes, and S. Maekawa, Equation-of-motion approach of spin-motive force, J. Appl. Phys. **109**, 07C735 (2011).

[3] G. Tatara, Effective gauge field theory of spintronics, Physica E **106**, 208 (2019).